

## Supporting Information

# Durable, Flexible Self-standing Hydrogel Electrolyte Enabling High-safety Rechargeable Solid-state Zinc Metal Battery

Qi Han<sup>a,b</sup>, Xiaowei Chi<sup>\*,a</sup>, Shuming Zhang<sup>a,b</sup>, Yunzhao Liu<sup>a,b</sup>, Biao Zhou<sup>a,b</sup>, Jianhua Yang<sup>a</sup>, Yu Liu<sup>\*,a</sup>

<sup>a</sup> Shanghai Institute of Ceramics, Chinese Academy of Sciences, Shanghai 200050, China

<sup>b</sup> University of Chinese Academy of Sciences, 19 Yuquan Road, Beijing 100049, China

This file includes characterization of the materials, supplementary figures S1-S18.

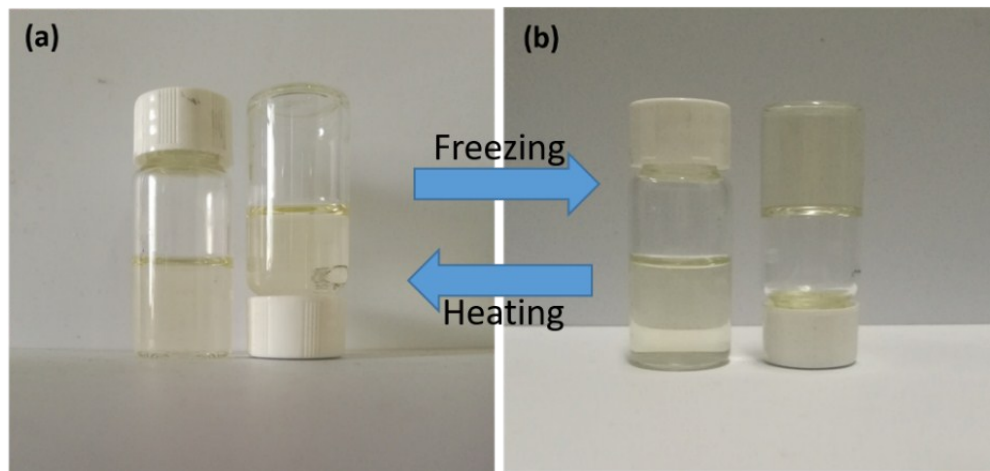


Fig. S1 Photographs of transformation of flowable gelation hydrogel electrolytes solution (gelatin dissolved in 0.5 M  $\text{Li}_2\text{SO}_4$  and 0.5 M  $\text{ZnSO}_4$  aqueous solution) to solidified GHEs: (a) after heating; (b) after freezing, illustrating the reversible flowability of gelation electrolyte.

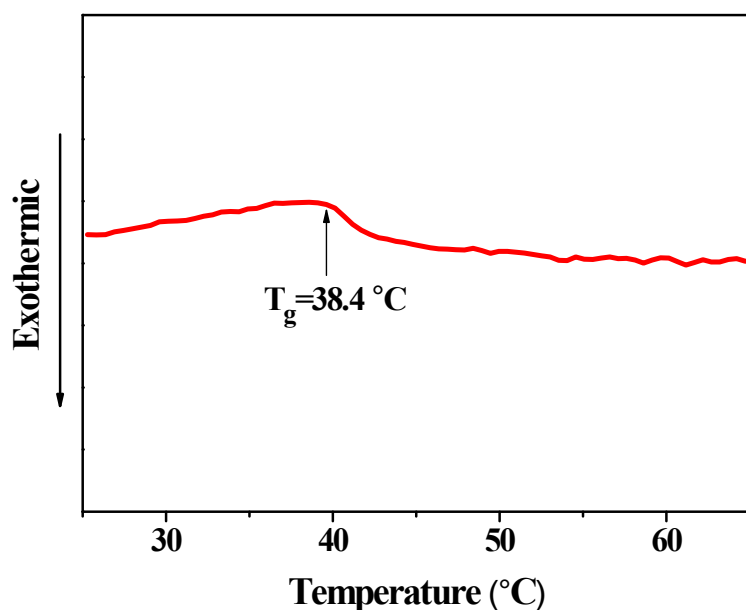


Fig. S2 DSC curve of the gelatin hydrogel electrolyte (GHE)

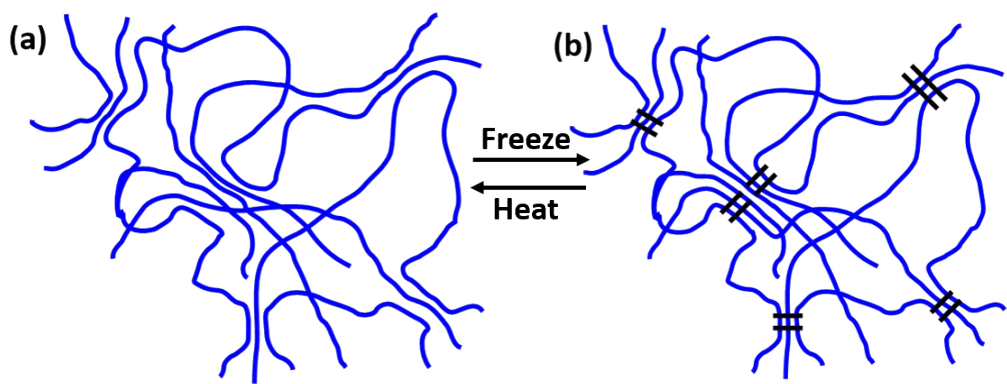


Fig. S3 Schematic diagram of the formation of network in GHEs. (a) Gelatin randomly dispersed in solution (upon heating), (b) Gelatin solidified to hydrogel (upon freezing).

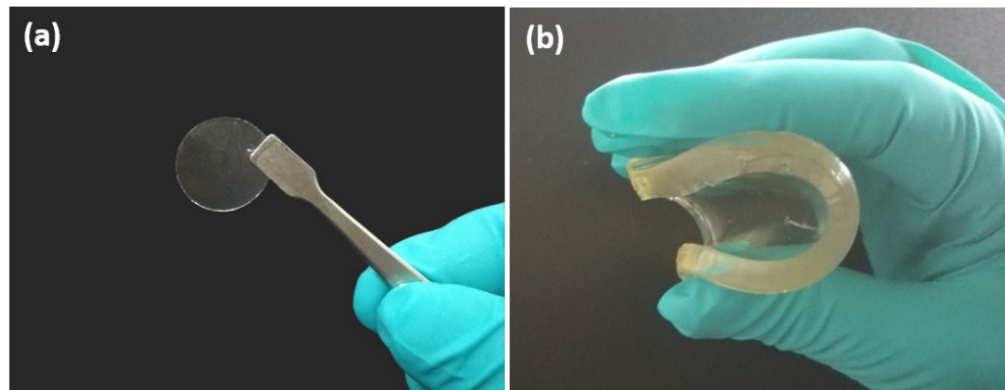


Fig. S4 Photographs of GHEs. (a) Gelatin electrolyte separator, (b) Thick gelatin electrolyte under bending condition.

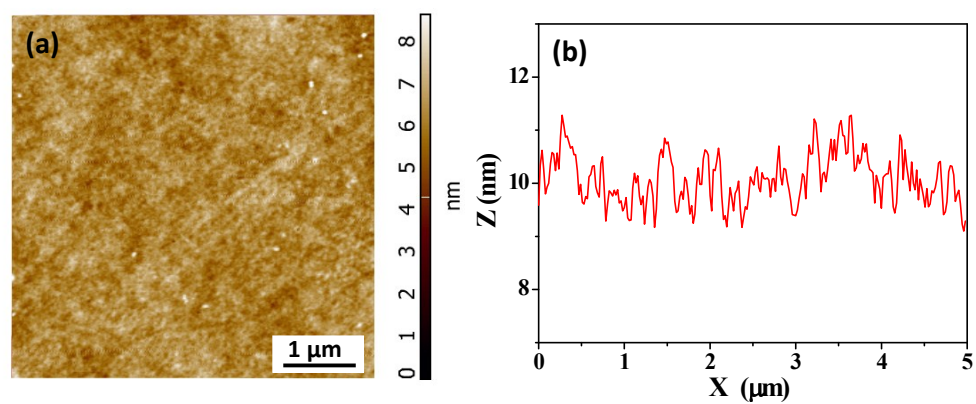


Fig. S5 (a) AFM image ( $5 \mu\text{m} \times 5 \mu\text{m}$ ) of the GHE film; (b) Height profile at  $Y=2.5 \mu\text{m}$  in the section of (a)

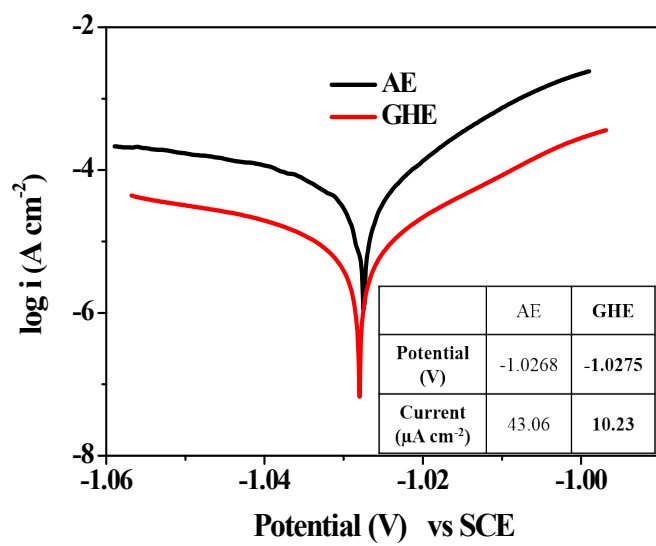


Fig. S6 Tafel plots of the Zn anode in AE and GHE

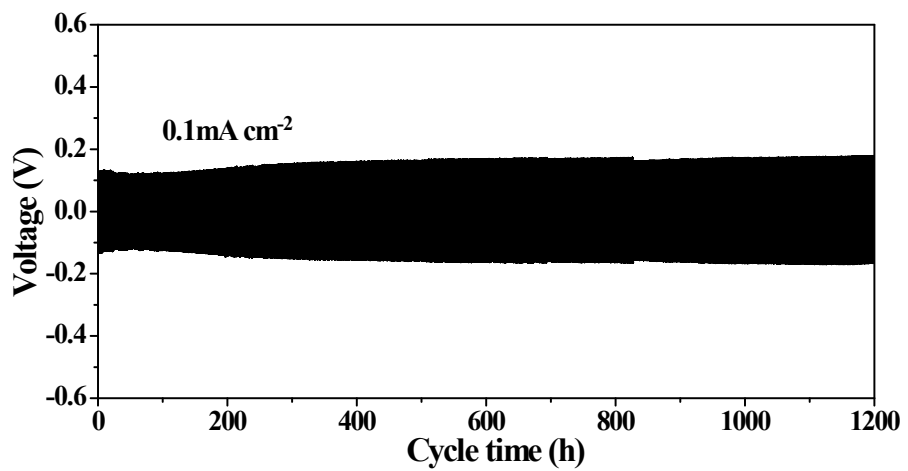


Fig. S7 Galvanostatic cycling tests of solid-state Zn/GHE/Zn symmetric cell at 0.1  $\text{mA cm}^{-2}$ .

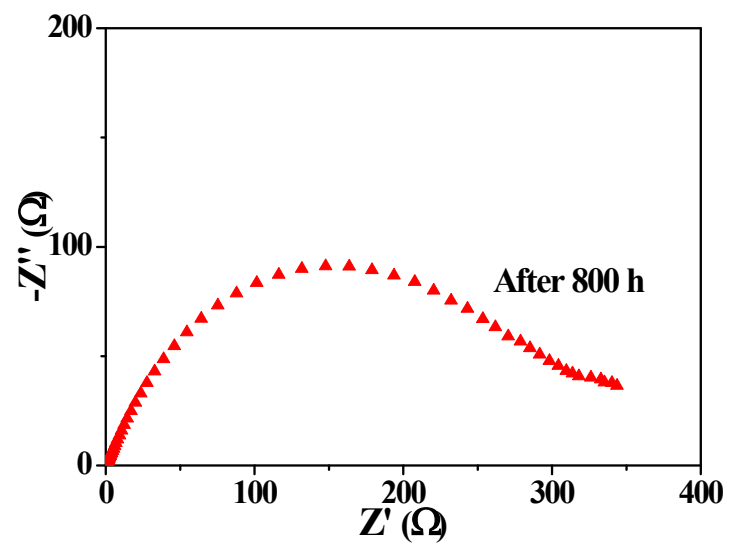


Fig. S8 EIS plot of Zn/GHE/Zn battery after cycling for 800 h.

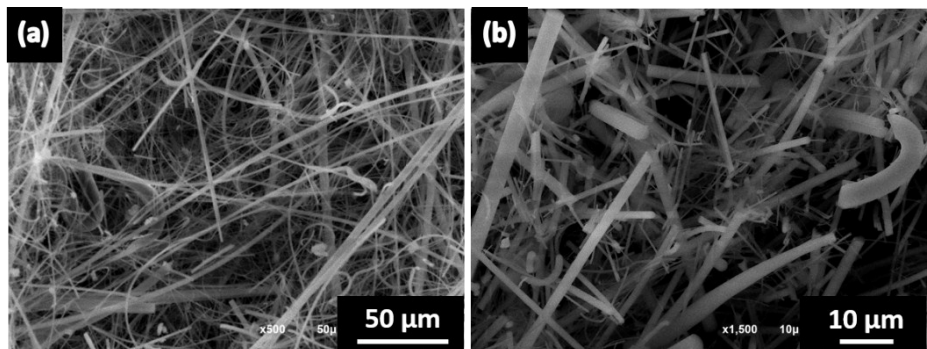


Fig. S9 SEM images of pristine AGM: (a) surface and (b) cross-section.

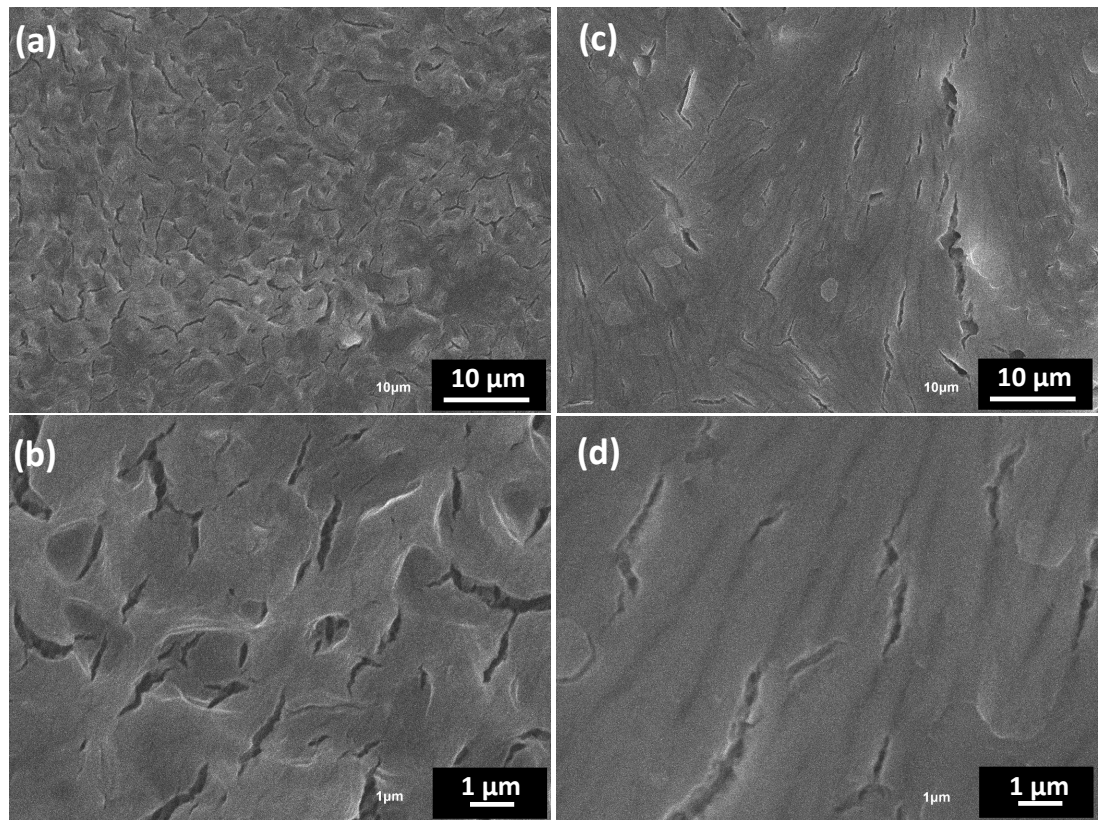


Fig. S10 SEM images of the GHEs before (a, b) and after (c, d) cycling in the symmetric cells

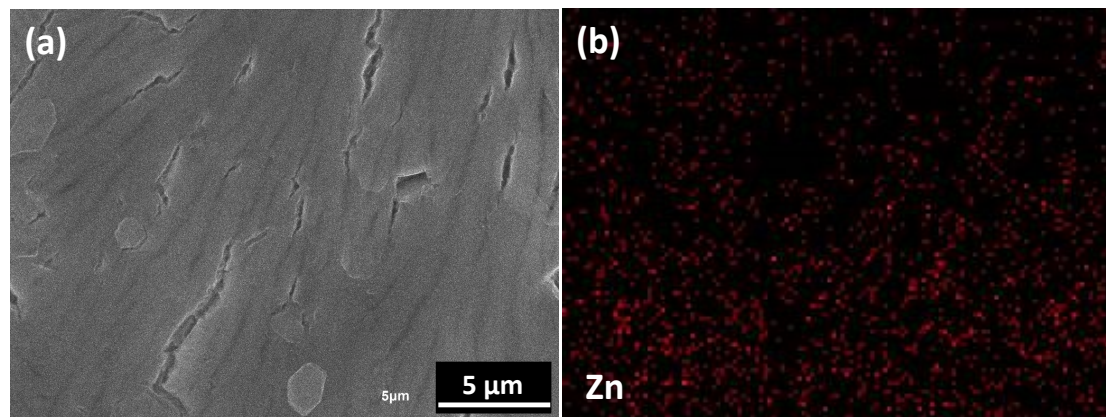


Fig. S11 (a) SEM image of the GHE after cycling; (b) mapping image of Zn element

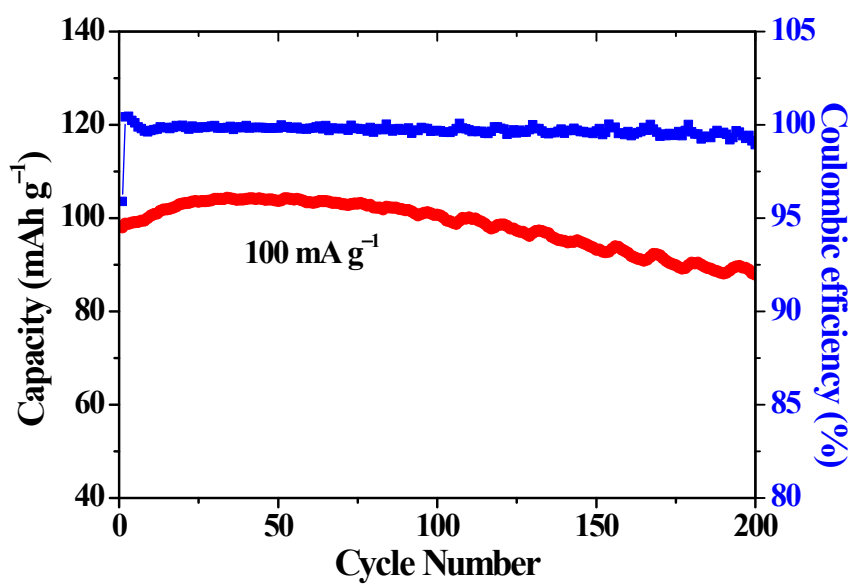


Fig. S12 Cycling performance of Zn/GHE/LMO full cells at a current density of 100  $\text{mA g}^{-1}$

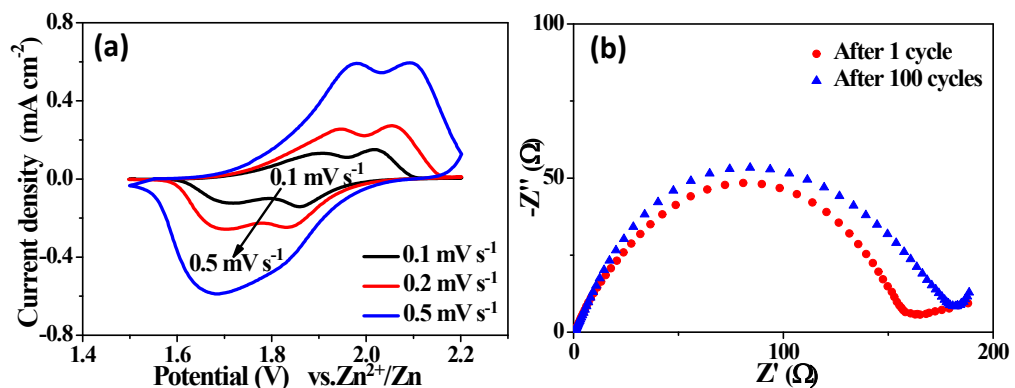


Fig. S13 Electrochemical characterizations of solid-state Zn/GHE/LMO batteries: (a) CV curves at different scanning rates; (b) EIS plots at different cycles.

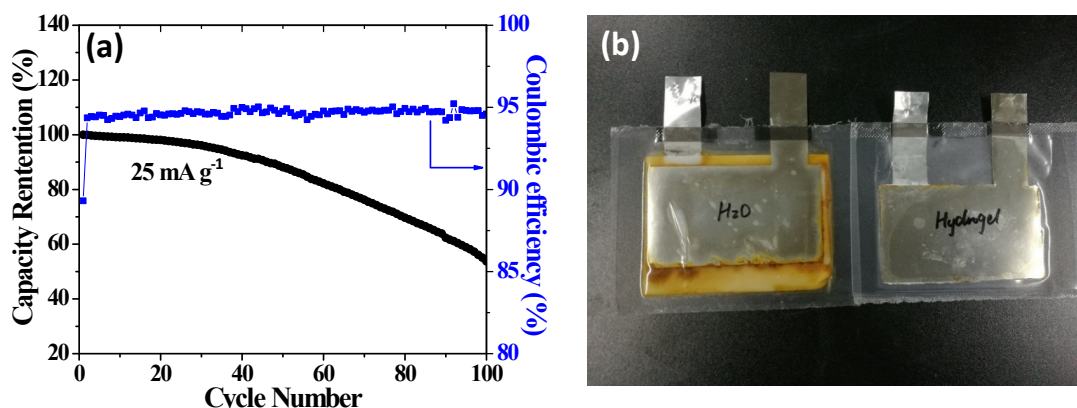


Fig. S14 (a) Cycle performance of Zn/LMO battery with AE at  $25 \text{ mA g}^{-1}$ ; (b) photographs of Zn/LMO batteries with AE and GHE after 100 cycles.

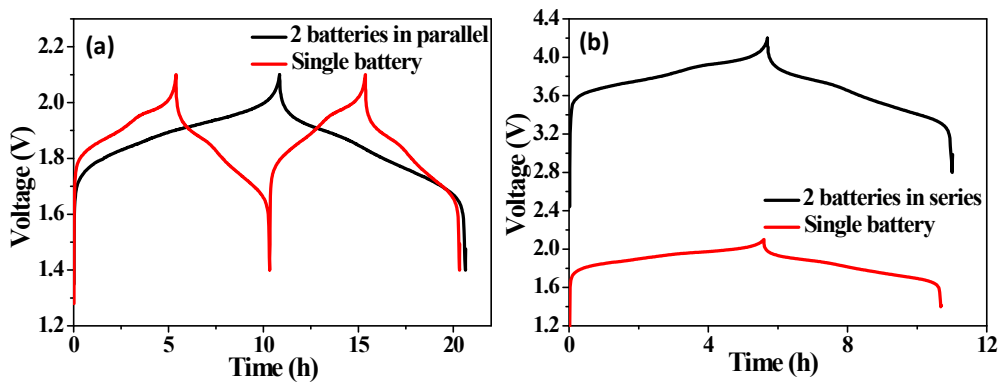


Fig. S15 Galvanostatic charge-discharge curves of two batteries connected in (a) parallel and (b) serial.

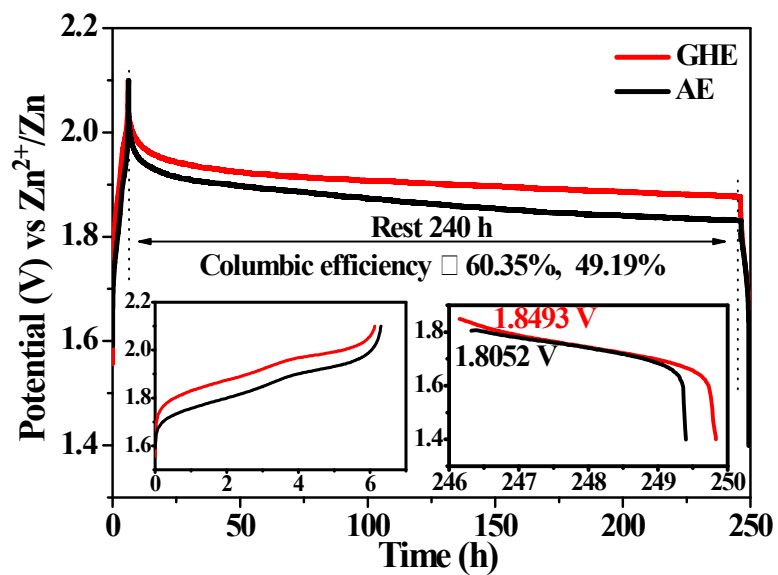


Fig. S16 Comparison of self-discharge performances of batteries based on AE and GHE.

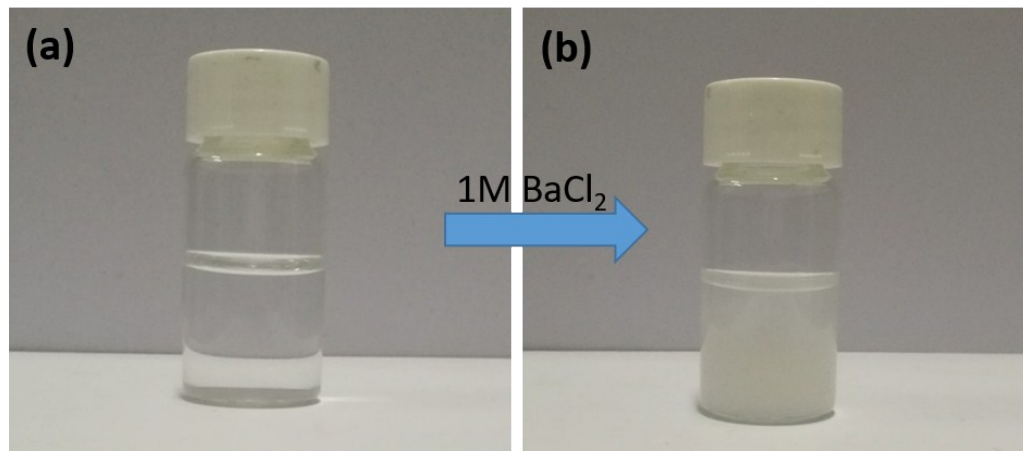


Fig. S17 Photograph of GHE soaked in pure water (a) and water added with several drops of 1 M BaCl<sub>2</sub> solution (b).

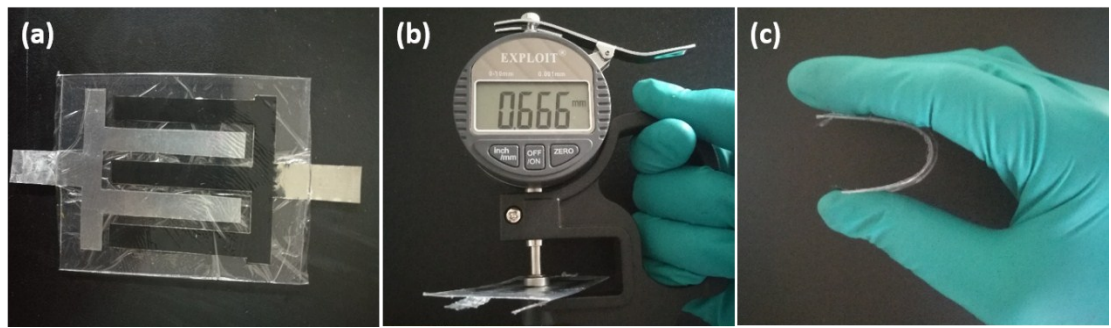


Fig. S18 Photographs of interdigitated Zn/GHE/LMO solid-state battery at different conditions.